JACS
JOURNAL OF THE AMERICAN CHEMICAL SOCIETY
Article
pubs.acs.org/JACS

Structural Control of $^1A_{2u}$-to-$^3A_{2u}$ Intersystem Crossing in Diplatinum(II,II) Complexes

Alec C. Durrell,[†] Gretchen E. Keller,[†] Yan-Choi Lam,[†] Jan Sýkora,[‡] Antonín Vlček, Jr.,*[,‡,§] and Harry B. Gray*[,†]

[†]Beckman Institute, California Institute of Technology, Pasadena, California 91125, United States

[‡]J. Heyrovský Institute of Physical Chemistry, Academy of Sciences of the Czech Republic, Dolejškova 3, CZ-182 23 Prague, Czech Republic

[§]School of Biological and Chemical Sciences, Queen Mary University of London, Mile End Road, London E1 4NS, United Kingdom

Supporting Information

ABSTRACT: Analysis of variable-temperature fluorescence quantum yield and lifetime data for per(difluoroboro)tetrakis(pyrophosphito)diplatinate(II) ($[Pt_2(\mu\text{-}P_2O_5(BF_2)_2)_4]^{4-}$, abbreviated Pt(pop-$BF_2$)), yields a radiative decay rate ($k_r = 1.7 \times 10^8$ s^{-1}) an order of magnitude greater than that of the parent complex, Pt(pop). Its temperature-independent and activated intersystem crossing (ISC) pathways are at least 18 and 142 times slower than those of Pt(pop) [ISC activation energies: 2230 cm^{-1} for Pt(pop-BF_2); 1190 cm^{-1} for Pt(pop)]. The slowdown in the temperature-independent ISC channel is attributed to two factors: (1) reduced spin−orbit coupling between the $^1A_{2u}$ state and the mediating triplet(s), owing to increases of LMCT energies relative to the excited singlet; and (2) diminished access to solvent, which for Pt(pop) facilitates dissipation of the excess energy into solvent vibrational modes. The dramatic increase in E_a is attributed to increased P-O-P framework rigidity, which impedes symmetry-lowering distortions, in particular asymmetric vibrations in the $Pt_2(P\text{-}O\text{-}P)_4$ core that would allow direct $^1A_{2u}$−$^3A_{2u}$ spin−orbit coupling.

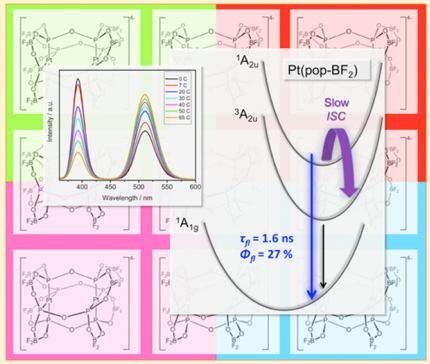

INTRODUCTION

Face-to-face d^8−d^8 complexes of Pt^{II}, Rh^I, and Ir^I possess truly remarkable spectroscopic, photophysical, and photochemical properties.[1−5] Electronic excitation from a metal−metal antibonding $(n-1)d\sigma^*$ orbital to an $np\sigma$ bonding orbital creates a net metal−metal bond (Figure 1); as a result, the metal−metal distance shrinks in both singlet and triplet ($^{1,3}d\sigma^*p\sigma$) excited states. In addition to strong phosphorescence, some of these complexes also show weak fluorescence, that, of the complexes studied to date, is most prominent for certain Ir^I−Ir^I complexes whose $^1d\sigma^*p\sigma$ states are able to reduce very low potential substrates.[6−9]

Tetrakis(μ-pyrophosphito)diplatinate(II), $[Pt_2(\mu\text{-}P_2O_5H_2)_4]^{4-}$, abbreviated Pt(pop), is the prototypal photoactive d^8−d^8 complex.[1] Its molecular structure (Figure 2, left) consists of two parallel PtP_4 square planar units held in a rigid configuration by four P-O-P bridges. The eight terminal P(O)(OH) groups, which are exposed to solvent, likely play a role in excited-state deactivation.[10,11] Pt(pop) shows very weak fluorescence from a $^1d\sigma^*p\sigma$ state that decays on a tens-of-picoseconds time scale with temperature- and solvent-dependent lifetimes,[10,11] and the corresponding triplet state exhibits intense green phosphorescence. Owing to its long lifetime (~10 μs)[12] and biradical character,[13,14] the $^3d\sigma^*p\sigma$ state reacts with a variety of substrates, including alcohols, hydrocarbons, alkylhalides,[2−5] DNA,[15] and metal complexes.[13,14,16] These reactions, which involve transfer of hydrogen or halogen atoms, can be viewed as photochemical oxidative-addition or inner-sphere electron-transfer processes.

The structures and dynamics of Pt(pop) $^{1,3}d\sigma^*p\sigma$ excited states have been extensively investigated.[10−12,17−20] Evidence that a Pt−Pt bond is formed upon $d\sigma^*\rightarrow p\sigma$ excitation has been extracted from Franck−Condon analysis of the vibronic structure associated with $d\sigma^*\rightarrow p\sigma$ absorption bands measured on single crystals at low temperatures. The Pt−Pt stretching frequency increases from 118 cm^{-1} in the ground state[21] to about 150 cm^{-1} in both singlet and triplet excited states,[12,17] and a stretching frequency of 155 cm^{-1} was found for the triplet by transient Raman spectroscopy.[21] A femtosecond time-resolved spectroscopic study[11] reported long-lasting (several ps) coherent oscillations of stimulated fluorescence with a 224 fs period corresponding to a 149 cm^{-1} stretching vibration, a finding that documented the harmonic nature of the $^1d\sigma^*p\sigma$ potential energy surface with respect to the Pt−Pt coordinate. The structure of the $^3d\sigma^*p\sigma$ state studied by time-resolved X-ray diffraction from a Pt(pop) single crystal showed a Pt−Pt bond contraction of 0.28 Å.[18] Arguably, the most detailed information on the $^3d\sigma^*p\sigma$ structure so far has been obtained by time-resolved X-ray absorption spectroscopy:[19] the appear-

Received: June 15, 2012
Published: August 6, 2012

   dx.doi.org/10.1021/ja305666b | J. Am. Chem. Soc. 2012, 134, 14201−14207

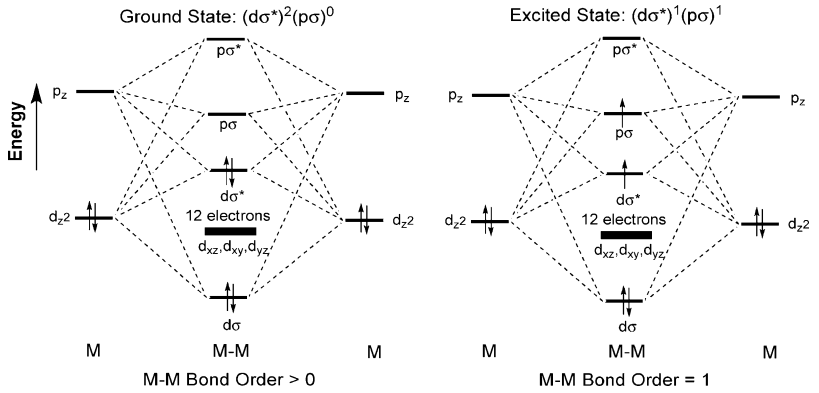

Figure 1. Electronic structures of d^8–d^8 complexes in the ground (left) and lowest triplet states (right).

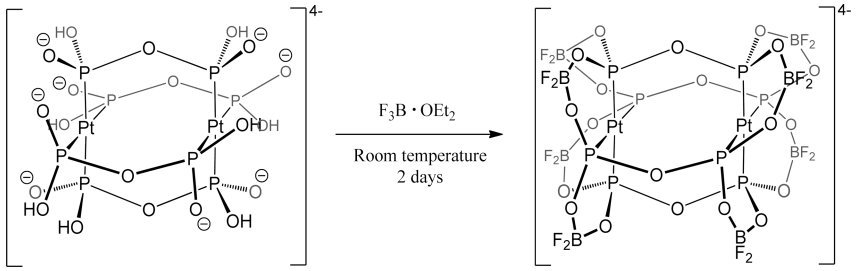

Figure 2. Conversion of Pt(pop) to Pt(pop-BF_2).

ance of a new pre-edge absorption feature upon excitation demonstrated creation of an electron vacancy ("hole") in the dσ* orbital; EXAFS analysis showed that the Pt–Pt distance contracts by 0.31 Å relative to that in the ground state; and the Pt–P bonds elongate by 0.01 Å, with Pt atoms shifting inward from the planes formed by the four phosphorus donor atoms, a structural picture that accords with excited-state DFT calculations.[22,23] Understanding and controlling relaxation pathways of electronically excited d^8–d^8 complexes remains a major challenge. In particular, several different mechanisms could account for singlet→triplet conversion (intersystem crossing).[10,11,24] It is of special interest that ^{1}dσ*pσ excited-state lifetimes vary from a few ps to almost 1 ns in d^8–d^8 Rh_2 complexes,[25] and that substantially different chemical reactivities have been found for singlet and triplet dσ*pσ states of Ir_2 derivatives.[6,25−27] A major goal of our work is to understand the factors that control the lifetimes of these energy-rich singlet states, as potentially they could be key players in photocatalysis and light-energy-harvesting schemes.

Pt(pop) offers very few opportunities for tuning its photobehavior by structural variations. Replacing each bridging −O− atom by a $-CH_2-$ group shortens the ^{3}dσ*pσ lifetime to 55 ns and accelerates photochemical atom- as well as electron-transfer reactions.[28,29] Since the terminal P(O)(OH) groups are the only other sites that can be derivatized, we set out to study the effects of substituting all eight pop hydrogen atoms by BF_2 groups, each linking oxygen atoms of two different pop ligands (Pt(pop-BF_2), Figure 2). Such "perfluoroboration" creates a rigid covalent cage around the Pt–Pt central motif, shields it from solvent and removes potentially energy-accepting −O−H···O− vibrations. Moreover, the ^{3}dσ*pσ state is expected to become a stronger oxidant, owing to the presence of electron-withdrawing BF_2 groups. We report here that ^{1}dσ*pσ to ^{3}dσ*pσ intersystem crossing in Pt(pop-BF_2) is dramatically slower than in Pt(pop), owing in part to BF_2-enhanced framework rigidity and electron-accepting properties that increase excitation energies to symmetry-lowering vibrational levels and higher electronic states that would allow spin-orbit mixing of the two dσ*pσ states.

RESULTS

The absorption spectrum of Pt(pop-BF_2) exhibits an intense band at 365 nm (ε = 37500 $M^{-1}\,cm^{-1}$) attributable to the dσ*→pσ ($^1A_{1g}\rightarrow{}^1A_{2u}$) transition; by comparison, Pt(pop) has a similar absorption feature at 372 nm (Figure 3 and Table 1).[12,17,30] The corresponding spin-forbidden dσ*→pσ transition ($^1A_{1g}\rightarrow{}^3A_{2u}$) gives rise to a ∼270× weaker band at 454 nm, virtually identical with that of Pt(pop).[12] Both complexes show a series of relatively weak UV bands. The 2100–3200 cm^{-1} high-energy shifts upon perfluoroboration are in line with the LMCT character indicated by TD-DFT calculations on Pt(pop).[22,23,31]

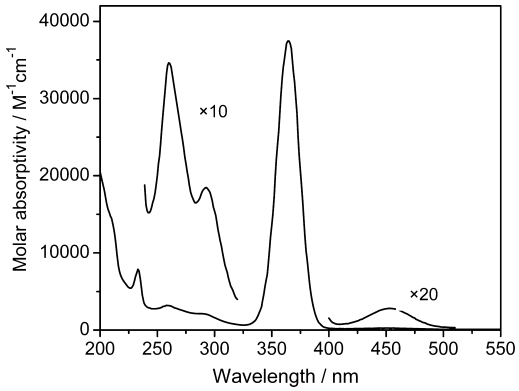

Figure 3. Absorption spectrum of Pt(pop-BF_2) in MeCN solution.

dx.doi.org/10.1021/ja305666b | J. Am. Chem. Soc. 2012, 134, 14201–14207

Table 1. Absorption and Emission Properties of Pt(pop-BF_2) and Pt(pop) in MeCN Solution

Pt(pop-BF_2)	Pt(pop)[a]	assignment[b]
Absorption, nm (ε, M^{-1} cm^{-1})		
233 (7880)	246 (3770)	LMCT[c]
260 (3180)	285 (2550)	LMCT[c]
291 (2110)	315 (1640)	LMCT[c]
365 (37500)	372 (33400)	$^1(d\sigma^*\rightarrow p\sigma)$ $^1A_{1g}\rightarrow{}^1A_{2u}$
454 (140)	454 (155)	$^3(d\sigma^*\rightarrow p\sigma)$ $^1A_{1g}\rightarrow{}^3A_{2u}$
Emission, nm (Lifetime at 21 °C)		
393 (1.6 ns)	398 (~8 ps)	$^1(p\sigma\rightarrow d\sigma^*)$ $^1A_{2u}\rightarrow{}^1A_{1g}$
512 (8.4 μs)	511 (9.4 μs)	$^3(p\sigma\rightarrow d\sigma^*)$ $^3A_{2u}\rightarrow{}^1A_{1g}$
Emission Stokes Shift, cm^{-1}		
1760	2230	fluorescence
2460	2500	phosphorescence

[a]Absorption data and emission lifetimes from ref 12, emission wavelengths from ref 32. [b]Based on refs 12, 22, and 23. [c]The principal excitations are directed to the pσ LUMO accompanied by smaller contributions from Pt-localized excitations.

The emission spectra of Pt(pop-BF_2) and Pt(pop) are very different in terms of the relative intensities of p$\sigma\rightarrow$dσ* fluorescence and phosphorescence. The spectrum of Pt(pop-BF_2) at room temperature shows intense $^3A_{2u}\rightarrow{}^1A_{2u}$ phosphorescence at 512 nm and equally strong fluorescence at 393 nm (Figure 4 and Table 1). Owing to phosphorescence quenching

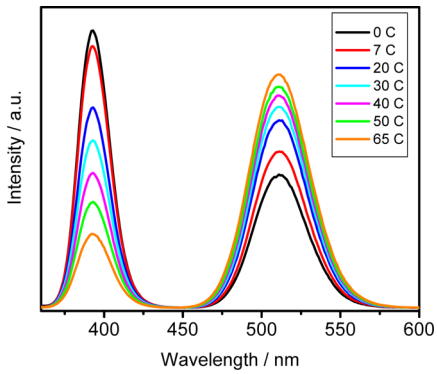

Figure 4. Temperature dependence of the emission spectrum of Pt(pop-BF_2) in MeCN solution. Excitation at 355 nm.

by traces of O_2, the intensity ratio of the two bands depends on sample preparation; a limiting phosphorescence:fluorescence peak-intensity ratio of 1.15 at 21 °C was obtained from a high-vacuum degassed solution. While Pt(pop) in MeCN also shows strong phosphorescence at 511 nm, the fluorescence at 398 nm is extremely weak,[12,32] as documented quantitatively by emission quantum yields: whereas room-temperature phosphorescence yields of the two complexes are comparable, the fluorescence yield is 3 orders of magnitude larger for Pt(pop-BF_2) than for Pt(pop) (2.7×10^{-1} and 1.5×10^{-4}, respectively).[12] The excitation spectra of Pt(pop-BF_2) measured at 405 and 512 nm are virtually identical and match perfectly the strong $^1A_{1g}\rightarrow{}^1A_{2u}$ absorption band at 363 nm (Figure S1); and the phosphorescence:fluorescence peak-intensity ratio is independent of excitation wavelength from 350 to 380 nm. Both the fluorescence band intensity and quantum yield decrease with increasing temperature, accompanied by a concomitant increase in phosphorescence intensity and yield (Figures 4 and S2, and Table S1). The total emission quantum yield of ca. 0.75 is temperature-independent, behavior that indicates direct conversion of the fluorescent state ($^1A_{2u}$) to the phosphorescent state ($^3A_{2u}$). This conclusion was confirmed by observing virtually identical single-exponential kinetics of fluorescence decay and phosphorescence rise, both occurring with a 1.6 ns lifetime (Figures 5, S3, and S4), that

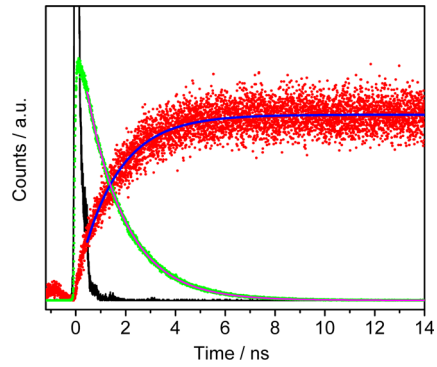

Figure 5. Phosphorescence rise at 512 nm (red) and fluorescence decay at 405 nm (green) of Pt(pop-BF_2) in MeCN, shown together with a 373 nm excitation-pulse profile (black). Measured using TCSPC. The blue and magenta curves are single-exponential fits in the 0.3−17.2 ns interval with lifetimes of 1.56 ± 0.02 and 1.58 ± 0.001 ns, respectively.

were measured at identical conditions except for detection wavelengths, 405 and 512 nm, respectively. This result was double-checked using two different techniques: time-correlated single photon counting (TCSPC) (373 nm, ~80 ps excitation, Figure 5) and streak camera (355 nm, 50 ps excitation, Figures S3 and S4). Our findings clearly demonstrate the presence of slow $^1A_{2u}\rightarrow{}^3A_{2u}$ intersystem crossing (ISC) in Pt(pop-BF_2) that occurs without any apparent intermediates.

The Pt(pop-BF_2) room-temperature fluorescence lifetime of 1.6 ns is about 100 times longer than the 8−18 ps values reported for Pt(pop) in MeCN[12] and similar solvents.[10,11] Figure 6 shows that the Pt(pop-BF_2) fluorescence decay is

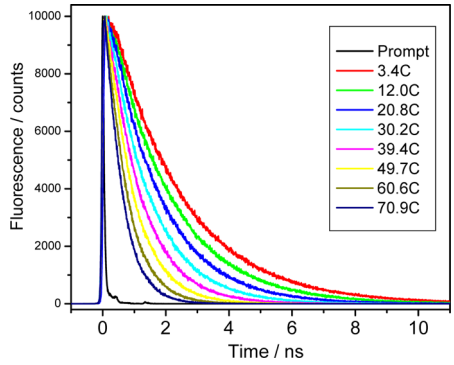

Figure 6. Temperature-dependent fluorescence decay of Pt(pop-BF_2) in MeCN solution. Excitation at 373 nm; emission detected at 405 nm.

strongly temperature-dependent, and the kinetics are predominantly single-exponential (lifetimes are collected in Table S2).[33] To analyze the temperature dependence of the fluorescence lifetime and quantum yield, we express the nonradiative decay rate constant k_{nr} as a sum of the ISC rate constant, k_{ISC}, and the nonradiative decay to the ground state, k_d (eq 1). Owing to the long fluorescence lifetime, the latter

dx.doi.org/10.1021/ja305666b | J. Am. Chem. Soc. 2012, 134, 14201−14207

cannot be *a priori* neglected as in the case of Pt(pop). k_{ISC} is assumed to follow Arrhenius-like behavior (eq 1), as proposed for Pt(pop).[10]

$$k_{nr} = k_d + k_{ISC} = k_d + \left(k_0 + \frac{A}{\sqrt{k_B T}} e^{-E_a/k_B T}\right) \quad (1)$$

The lifetime and quantum yield are then given by eqs 2 and 3, respectively.

$$\frac{1}{\tau} = k_r + k_{nr} = k_r + k_d + k_0 + \frac{A}{\sqrt{k_B T}} e^{-E_a/k_B T} \quad (2)$$

$$\frac{1}{\phi_{fl}} = 1 + \frac{k_{nr}}{k_r} = 1 + \frac{k_d + k_0}{k_r} + \frac{A}{k_r\sqrt{k_B T}} e^{-E_a/k_B T} \quad (3)$$

Fitting the experimental data to these equations gives $k_r + k_d + k_0 = (2.55 \pm 0.07) \times 10^8$ s^{-1}; $A = (3.0 \pm 0.2) \times 10^{14}$ cm$^{1/2}$ s^{-1}; $E_a = 2229 \pm 20$ cm^{-1} for the lifetime, and $(k_d+k_0)/k_r = 0.6 \pm 0.1$; $A/k_r = (1.7 \pm 0.5) \times 10^6$ cm$^{1/2}$; $E_a = 2233 \pm 75$ cm^{-1} for the quantum yield (Figure 7). The activation energies from

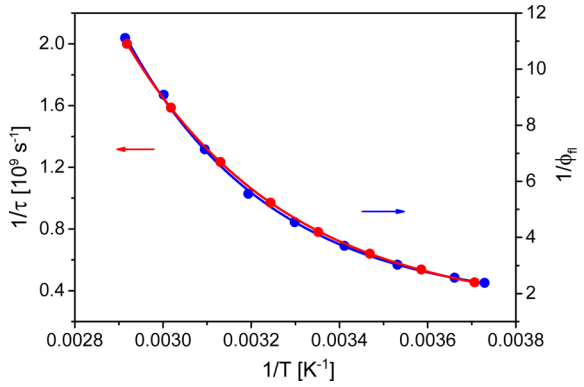

Figure 7. Temperature dependence of Pt(pop-BF_2) fluorescence lifetime (red, left scale) and quantum yield (blue, right scale) fitted to eqs 2 and 3, respectively. Data from Tables S1 and S2.

these two fits are virtually identical, in accordance with eqs 2 and 3 and the assumption of *T*-independent k_r and k_d (*T*-dependent k_d would require two exponential terms, for which we have no evidence). Neglecting k_d, the radiative rate constant (k_r) can be estimated (Table S2) to be 1.7×10^8 s^{-1}, which is ca. 8× larger than that of Pt(pop) (2×10^7 s^{-1}); and 8.5×10^7 s^{-1} is the rate of T-independent nonradiative decay ($k_d + k_0$).

Pt(pop-BF_2) phosphorescence decay occurs with a lifetime of 8 μs that is temperature-independent within the measurement accuracy over the 0−70 °C range (measured in a high-vacuum (4×10^{-5} mbar) freeze−pump−thaw degassed MeCN solution). This value is comparable to the phosphorescence lifetime of Pt(pop), 9.4 μs.[12]

DISCUSSION

The presence of a long-lived strongly emissive singlet excited state together with a strongly phosphorescent triplet are the distinctive photophysical features of Pt(pop-BF_2). The $^1A_{2u} \rightarrow {}^3A_{2u}$ ISC in Pt(pop) has been studied in detail both experimentally[10,11] and theoretically,[24] but the mechanism is still open to debate. Herein, we will concentrate on the dramatic ISC slowdown caused by perfluoroboration of the complex. In both Pt(pop) and Pt(pop-BF_2), ISC proceeds by a two-channel mechanism, eq 1: the corresponding kinetics parameters for the two complexes are listed in Table 2.

Table 2. Decay Kinetics Parameters for the $^1A_{2u}$ Excited States of Pt(pop-BF_2) and Pt(pop)

	Pt(pop-BF_2)	Pt(pop)[a]
k_r	1.7×10^8 s^{-1}	2×10^7 s^{-1}
k_0	$<8.5 \times 10^7$ s^{-1} [c]	1.5×10^9 s^{-1}
A	3.0×10^{14} cm$^{1/2}$ s^{-1}	2.6×10^{14} cm$^{1/2}$ s^{-1}
E_a	2230 cm^{-1}	1190 cm^{-1}
$A/\sqrt{(k_B \times 293)}$	2.1×10^{13} s^{-1}	1.8×10^{13} s^{-1}
$\exp[-E_a/(k_B \times 293)]$	1.749×10^{-5}	2.893×10^{-3}
k_{nr} [b]	4.7×10^8 s^{-1}	5.4×10^{10} s^{-1}

[a] k_r from ref 12, measured in MeCN. Other parameters from ref 10, measured in a 2-MeTHF/propionitrile mixture. [b] For Pt(pop-BF_2), see Table S2. For Pt(pop): calculated from the parameters reported in the table: k_0, A, E_a. [c] The value corresponds to $k_0 + k_d$ and thus represents an upper limit of k_0. We assume that k_d is negligibly small.

Compared with Pt(pop), the temperature-independent and the thermally activated ISC pathways in Pt(pop-BF_2) are slowed ca. 18 and 142 times (at 20 °C), respectively. The corresponding mechanisms are discussed below, starting with the T-independent ISC.

We assume that ISC rates are given by eq 4, where H_{SO} is the spin−orbit (SO) operator and FC is the Franck−Condon factor that accounts for the thermally weighted overlap between vibrational wave functions of the initial and final states.

$$k_{ISC} \propto \langle {}^1A_{2u}|H_{SO}|{}^3A_{2u}\rangle^2 FC \quad (4)$$

Temperature-independent $^1A_{2u} \rightarrow {}^3A_{2u}$ direct tunneling (k_0) is about 18 times slower in Pt(pop-BF_2) than Pt(pop). Note that direct ISC between states of identical symmetries is allowed only in point groups where at least one of the rotation components belongs to the totally symmetric representation [it is forbidden in the D_{4h} group of the $Pt_2(P\text{-}O\text{-}P)_4$ core (i.e., $\langle {}^1A_{2u}|H_{SO}|{}^3A_{2u}\rangle = 0$), but it is allowed in C_{4h}, C_{2h}, or C_2]. However, even in D_{4h}, ISC could become partially allowed by SO mixing with higher triplet states[34−36] and/or through a spin-vibronic mechanism.[24,37−39] In particular, SO coupling between $^1A_{2u}$ and ^3E_u states is symmetry allowed, admixing triplet character into $^1A_{2u}$ that then can undergo internal conversion to E_u and/or A_{1u} spin components of the $^3A_{2u}$ state.[24] In both Pt(pop-BF_2) and Pt(pop), the higher-lying ^3E_u LMCT is the likely coupling state. As documented by UV spectra, perfluoroboration raises the energy of LMCT states relative to $^1A_{2u}$, thereby diminishing the $^1A_{2u}-{}^3E_u$ coupling, which in turn slows ISC (eq 5).

$$k_{ISC} \propto \frac{\langle {}^1A_{2u}|H_{SO}|{}^3E_u\rangle^2}{E({}^3E_u) - E({}^1A_{2u})} FC \quad (5)$$

Irrespective of the details of the indirect spin−orbit interaction, the ISC tunneling pathway also is expected to be disfavored in Pt(pop-BF_2) because of the smaller FC factor. Since the $^1A_{2u}$ and $^3A_{2u}$ states largely behave as two imbedded Pt−Pt harmonic oscillators,[11] the overlap between their vibrational wave functions is small and solvent vibrations gain in importance as energy-accepting modes, as was clearly manifested by the strong solvent dependence of the Pt(pop) k_0.[10] As BF_2 groups are much bulkier than −O−H···O− units, they will weaken direct interactions between the solvent and

dx.doi.org/10.1021/ja305666b | J. Am. Chem. Soc. 2012, 134, 14201−14207

terminal P(=O)O groups as well as with the Pt atoms. Perfluoroboration thus diminishes the ability of the solvent to provide vibrational coupling between the singlet and triplet states, which is required to accept the ca. 5650 cm^{-1} energy released during ISC.

The increase from 1190 to 2230 cm^{-1} in the ISC activation energy is the main factor responsible for the dramatically longer singlet lifetime of Pt(pop-BF_2), as it slows down the activated ISC pathway ca. 140× at 20 °C (Table 2) relative to Pt(pop). For Pt(pop), it was proposed[10] that the activated pathway involves thermal population of a higher-lying $d\sigma^* \rightarrow d_{x^2-y^2}$ $^3B_{2u}$ state from $^1A_{2u}$, followed by fast $^3B_{2u}$ decay to $^3A_{2u}$. We suggest, however, that ^3E_u LMCT is a much more likely candidate for the intermediate state, as $^3B_{2u}$ is not coupled to $^1A_{2u}$ by first-order SO, and it lies at much higher energy than thought previously.[22,23,31] Perfluoroboration, which shifts LMCT states to higher energies (Table 1), should raise the $^1A_{2u} - {}^3E_u$ barrier, in line with experiment. Although thermal population of an intermediate electronic state is the conventional explanation of T-dependent excited-state nonradiative decay in transition metal complexes, we have no evidence that would support such a mechanism in the cases of Pt(pop) and Pt(pop-BF_2). Indeed, a recent ultrafast study of vibrational coherence in the Pt(pop) $^1A_{2u}$ state demonstrated that its potential energy surface has harmonic character, which would suggest the absence of an avoided crossing with any low-lying intermediate state.[11] For the same reason, it would be hard to justify an assumption of strong coupling (i.e., surface crossing) between $^1A_{2u}$ and $^3A_{2u}$, whose potential energy surfaces appear to be "embedded", owing to the very similar structures of these states. (Note, however, that the Stokes shift is larger for phosphorescence than fluorescence, indicating that $^3A_{2u}$ is more distorted with respect to the ground state than $^1A_{2u}$.)

An alternative explanation that we favor is that thermal population of higher levels of certain vibrational modes provides stronger $^1A_{2u} - {}^3A_{2u}$ SO coupling than that in the $^1A_{2u}$ ground vibrational state. In other words, activated ISC would not occur from the $\nu = 0$ level of $^1A_{2u}$, but from higher levels of appropriate asymmetric vibrations that are in resonance with target-state ($^3A_{2u}$) vibrational levels. It follows that the most efficient ISC activation would be associated with thermal excitation of deformation modes that lower the symmetry to C_{4h}, C_{2h}, or C_2, allowing first-order $^1A_{2u}$–$^3A_{2u}$ SO coupling. Since the states involved in ISC are strongly localized along the Pt–Pt bond, it is not expected that symmetry lowering due to changes in the mutual orientation of peripheral BF_2 (or, in Pt(pop), −O−H···O− groups) would strongly affect the ISC rate. Instead, the distortion would come from excitation of asymmetric vibrations of the $Pt_2(P\text{-}O\text{-}P)_4$ core. Such distortions also could induce mixing between $^{1,3}d\sigma^*p\sigma$ and LMCT states, thereby facilitating indirect SO coupling as well. The increase of the apparent activation energy upon perfluoroboration is attributable to the rigidity of covalent −BF_2− linkages that increases the energy of activating vibrational modes, so that higher temperatures are required for distortion amplitudes sufficient to induce SO coupling. If this explanation is correct, the fluorescence lifetime should depend on the temperature according to eq 6 that assumes Boltzmann equilibrium between the emissive and a higher-lying deactivating state.[40]

$$\frac{1}{\tau} = \frac{k_0 + k_1 \exp(-\Delta E/k_B T)}{1 + \exp(-\Delta E/k_B T)} \quad (6)$$

Indeed, a near perfect correlation has been found (Figure S5), with the following parameters: $k_0 = (2.52 \pm 0.07) \times 10^8$ s^{-1}, $k_1 = (1.18 \pm 0.09) \times 10^{13}$ s^{-1}, and $\Delta E = 2110 \pm 21$ cm^{-1}, implying sub-ps resonant ISC from a state 2110 cm^{-1} above the zero vibrational level of $^1A_{2u}$. If the deactivating state is of vibrational origin, population of $\nu = 4-6$ levels of skeletal modes would be required. In reality, simultaneous thermal excitation of several different modes could contribute and the experimental ΔE value should be viewed as an average activation energy.

Long-lived singlet excited states are rare for transition-metal complexes. For example, the ^{1}MLCT states of $[M^{II}(bpy)_3]^{2+}$ (M = Fe, Ru) decay to the corresponding triplets in less than 30 fs,[41,42] while 80–150 fs lifetimes have been reported for the singlet excited states of Re^I carbonyl-diimine sensitizers.[43−45] A dimeric platinum(II) complex [Pt(2-phenylpyridine)(μ-^{t}Bu$_2$-pyrazolate)]$_2$ with a $d\sigma^* \rightarrow$ppy ^{1,3}MMLCT states shows an ultrafast 145 fs ISC.[46] Besides Pt(pop), ps-lived singlet states have been observed at ambient temperatures for d^8-d^8 complexes of Rh and Ir.[6,25,47−49] In particular, $[Rh_2(1,3\text{-diisocyanopropane})_4]^{2+}$ exhibits room-temperature solution fluorescence and phosphorescence lifetimes of 1.3 ns and 8.3 μs, respectively, but the fluorescence quantum yield is only 0.07.[48] Other examples of long-lived excited singlets include quadruply bonded metal–metal dimers such as $Mo_2X_4(PR_3)_4$ (X = Cl, Br, I; R = Me, n-Bu) and $[Re_2X_8]^{2-}$ (X = Cl, Br); these complexes possess $^1\delta\delta^*$ states that have 16–140 ns lifetimes, with $^3\delta\delta^*$ states that are largely bypassed during $^1\delta\delta^*$ decay.[50,51] The $^1\delta\delta^*$ lifetimes reported for these complexes thus correspond to internal conversion directly to the ground state, the ISC to $^3\delta\delta^*$ being much slower, owing to the very large singlet–triplet splitting and vanishing $^1\delta\delta^*$–$^3\delta\delta^*$ SO coupling. $^3\delta\delta^*$ states have been detected only very recently by time-resolved IR spectroscopy of $M_2(O_2CR)_4$ complexes (M = Mo, W; R = Bu), for which lifetimes of 40 and 50 ps were attributed to ^{1}MLCT$\rightarrow{}^3\delta\delta^*$ and $^1\delta\delta^* \rightarrow {}^3\delta\delta^*$ ISC processes, respectively.[52] And $M_2(O_2CR)_4$ complexes with electron-accepting substituents R show weakly emissive $\delta \rightarrow \pi^*(O_2CR)$ ^{1}MLCT states that decay to the corresponding nonemissive triplets in 4 to 20 ps.[53,54] Among mononuclear complexes, picosecond ISC times have been reported for ^{1}MLCT states of flattened-tetrahedral complexes of Cu^I (13–16 ps)[37] and Pt^0 (3.2 ps).[55] Symmetry-forbidden first-order SO coupling between optically excited singlet and lowest triplet states is a common feature for all systems with ps-ns singlet lifetimes. Still, "forbidden" ISC in metal complexes is many orders of magnitude faster than ISC in organic molecules. Theories of spin-vibronic coupling and ISC rates have been elaborated in detail for organic systems that are characterized by very weak SO interactions and small structural perturbations.[37−39] Understanding the dynamics of SO-coupled states of metal-containing molecules and developing systems capable of harvesting singlet excitation energy are major goals of contemporary transition-metal photophysics.[36]

■ CONCLUDING REMARKS

We have shown that modifying all eight P–O–H···O–P peripheral sites strongly affects Pt(pop) photophysical properties. Pt(pop-BF_2), which possesses an unusually long-lived singlet excited state, displays very intense fluorescence *and*

phosphorescence. The singlet-to-triplet ISC is slow, 1.6 ns at room temperature. Nonradiative decay to the ground state is far less important. We can conclude that the dramatic ISC slowing relative to Pt(pop) is attributable to the electron-withdrawing power of BF_2, which raises pop→pσ LMCT relative to dσ^*→pσ state energies and diminishes indirect SO coupling, and a much more rigid structure, owing to covalent $-BF_2-$ bridges linking the pop ligands that also shield the $Pt_2(P\text{-}O\text{-}P)_4$ core from solvent. The distinctive photophysical features of Pt(pop-BF_2) provide a unique opportunity to investigate independently the structures, dynamics and reactivities of both singlet and triplet dσ^*→pσ excited states in the same molecule. We expect that long-lived vibrational coherence will be observed for the singlet state, and that excited-state reactivity could reflect the asymptotic zwitterionic character of the singlet[56,57] and the radical-like behavior of the triplet.[2,3,5,13,14]

EXPERIMENTAL SECTION

Pt(pop-BF_2) Synthesis and Structure. Details of the synthesis of $[Bu_4N]_4[Pt_2(\mu\text{-}P_2O_5(BF_2)_2)_4]$ (Pt(pop-BF_2)) are given in the Supporting Information. Briefly, tetrabutylammonium Pt(pop) was stirred under a dry argon atmosphere in boron trifluoride diethyl etherate for two days at room temperature. The solvent was removed by vacuum distillation, and the product was washed with THF. Samples suitable for photophysical studies were twice recrystallized by diffusion of diethylether into a MeCN solution of the compound. A crystallographic study[58] showed that the structure of Pt(pop-BF_2) is very similar to that of Pt(pop), containing two parallel PtP_4 planes. The Pt−Pt (2.8895), Pt−P (2.294), and P−O (1.614 Å) bonds are slightly shorter than those in Pt(pop) (2.9203, 2.3360, 1.638 Å).[59]

All Pt(pop-BF_2) samples for spectroscopic studies were prepared under anhydrous, oxygen-free conditions using drybox and/or Schlenk techniques. Additional freeze−pump−thaw degassing at high vacuum (4×10^{-5} mbar) was used for some of the emission experiments. Anhydrous acetonitrile was obtained from Acros Organics (Extra Dry, AcroSeal) or Aldrich (SureSeal). Variable-temperature experiments were performed using a Peltier-cooled circulating water bath.

Electronic Absorption Spectroscopy. UV−vis absorbance spectra were recorded on an Agilent 8453 UV−vis spectrometer using a pure solvent as the background.

Steady-State Emission. Steady-state emission spectra were recorded on a Jobin Yvon Spex Fluorolog-3-11. A 450-W xenon arc lamp was used as the excitation source with a single monochromator providing wavelength selection. Right-angle light emission was sorted using a single monochromator and fed into a Hamamatsu R928P photomultiplier tube with photon counting. Short and long pass filters were used where appropriate. Spectra were recorded on Datamax software. Both fluorescence and phosphorescence quantum yields were measured from optically dilute MeCN solutions using anthracene in EtOH as a standard.

Time-Resolved Luminescence. Fluorescence decay and phosphorescence rise were measured using two independent experimental setups: time correlated single photon counting (TCSPC) and a streak camera in a photon-counting mode. Both techniques produced virtually identical results.

TCSPC: An IBH 5000 U instrument equipped with a cooled Hamamatsu R3809U-50 microchannel plate photomultiplier was used. Samples were excited at 373 nm with an IBH NanoLED-03 diode laser (~80 ps fwhm, repetition rate 500 kHz). For fluorescence decay measurements, the emission monochromator was set to 405 ± 4 nm, preceded by a 390 nm long-pass cutoff filter to remove all stray excitation light. Phosphorescence rise kinetics were measured with the monochromator set at 512 ± 16 nm, in combination with a 450 nm long-pass cutoff filter that removed both the excitation stray light and residual fluorescence. Magic angle between the excitation and emission polarization directions was used for all experiments. The temporal resolution was 2.89 ps/channel. Temperature dependence of the fluorescence decay was measured with a 7.07 ps/channel resolution. Data were analyzed using IBH Datastation2 or Microcal Origin 7.1 software. The sample solutions were prepared in a controlled-atmosphere (0.3 ppm O_2) glovebox (Jacomex) using dry, degassed MeCN Aldrich SureSeal. Additional high-vacuum (4×10^{-5} mbar) freeze−pump−thaw degassing was applied on solutions for all phosphorescence and some of the fluorescence measurements.

Streak camera in photon-counting mode: samples were excited with 50 ps pulses at 355 nm from the third harmonic of a regeneratively amplified mode-locked Nd:YAG laser (Vanguard 2000-HM532; Spectra-Physics) operating at 10 Hz. Emission was collected on a picosecond streak camera (Hamamatsu C5680 in photon-counting mode); singlet emission was selected by a 400−415 nm bandpass filter and triplet rise selected with a 500 nm long-pass filter. The measurements were made under magic-angle conditions and data were collected over a 50 ns sweep range with 8000 exposures.

To monitor triplet emission (phosphorescence), samples were excited at 355 nm with 8-ns pulses from the third harmonic of a Q-switched Nd:YAG laser (Spectra-Physics Quanta-Ray PRO-Series) operating at 10 Hz. Emission wavelengths were selected using a double monochromator (Instruments SA DH-10) with 1 mm slits. Luminescence was detected with a photomultiplier tube (PMT, Hamamatsu R928). The PMT current was amplified and recorded with a transient digitizer (Tektronix DSA 602). Short- and long-pass filters were employed to remove scattered excitation light. Decay traces were averaged over 500 laser pulses. Instruments and electronics in this system were controlled by software written in LabVIEW (National Instruments). Data manipulation was performed and plotted using MATLAB R2008a (Mathworks, Inc.). Some measurements were performed using TCSPC set as described above, except for the repetition rate (10 kHz) and time resolution (121.44 ps/channel).

ASSOCIATED CONTENT

Supporting Information

Synthesis, emission and excitation spectra, temperature-dependent fluorescence and phosphorescence quantum yields and lifetimes, as well as the time-resolved fluorescence decay and phosphorescence rise of Pt(pop-BF_2) measured by streak camera. This material is available free of charge via the Internet at http://pubs.acs.org.

AUTHOR INFORMATION

Corresponding Author

a.vlcek@qmul.ac.uk; hbgray@caltech.edu

Notes

The authors declare no competing financial interest.

ACKNOWLEDGMENTS

We thank Renske van der Veen for interesting discussions. Research at Caltech was supported by the NSF Center for Chemical Innovation (Powering the Planet CHE-0802907 and CHE-0947829) and CSER (Gordon and Betty Moore Foundation). Work at the J. Heyrovský Institute was funded by the Czech Ministry of Education program KONTAKT (grant ME10124).

REFERENCES

(1) Roundhill, D. M.; Gray, H. B.; Che, C. M. *Acc. Chem. Res.* **1989**, *22*, 55−61.

(2) Smith, D. C.; Gray, H. B. *Coord. Chem. Rev.* **1990**, *100*, 169−181.

(3) David, C. Smith; Gray, H. B. In *The Challenge of d and f Electrons*; ACS Symposium Series *307*; American Chemical Society: Washington, DC, 1989; pp 356−365.

(4) Marshall Janet, L.; Stiegman Albert, E.; Gray Harry, B. In *Excited States and Reactive Intermediates*; ACS Symposium Series *307*; American Chemical Society: Washington, DC, 1986; pp 166−176.

(5) Sweeney, R. J.; Harvey, E. L.; Gray, H. B. *Coord. Chem. Rev.* **1990**, *105*, 23−34.
(6) Fox, L. S.; Kozik, M.; Winkler, J. R.; Gray, H. B. *Science* **1990**, *247*, 1069−1071.
(7) Fox, L. S.; Marshall, J. L.; Gray, H. B.; Winkler, J. R. *J. Am. Chem. Soc.* **1987**, *109*, 6901−6902.
(8) Farid, R. S.; Chang, I.-J.; Winkler, J. R.; Gray, H. B. *J. Phys. Chem.* **1994**, *98*, 5176−5179.
(9) Gray, H. B.; Winkler, J. R.; Wiedenfeld, D. *Coord. Chem. Rev.* **2000**, *200−202*, 875−886.
(10) Milder, S. J.; Brunschwig, B. S. *J. Phys. Chem.* **1992**, *96*, 2189−2196.
(11) van der Veen, R. M.; Cannizzo, A.; van Mourik, F.; Vlček, A., Jr.; Chergui, M. *J. Am. Chem. Soc.* **2011**, *133*, 305−315.
(12) Stiegman, A. E.; Rice, S. F.; Gray, H. B.; Miskowski, V. M. *Inorg. Chem.* **1987**, *26*, 1112−1116.
(13) Vlček, A., Jr.; Gray, H. B. *Inorg. Chem.* **1987**, *26*, 1997−2001.
(14) Vlček, A., Jr.; Gray, H. B. *J. Am. Chem. Soc.* **1987**, *109*, 286−287.
(15) Kalsbeck, W. A.; Gingell, D. M.; Malinsky, J. E.; Thorp, H. H. *Inorg. Chem.* **1994**, *33*, 3313−3316.
(16) Kirk, A. D.; Cai, L.-Z. *Inorg. Chem.* **1998**, *37*, 1051−1059.
(17) Rice, S. F.; Gray, H. B. *J. Am. Chem. Soc.* **1983**, *105*, 4571−4575.
(18) Kim, C. D.; Pillet, S.; Wu, G.; Fullagar, W. K.; Coppens, P. *Acta Crystallogr. A* **2002**, *58*, 133−137.
(19) van der Veen, R. M.; Milne, C. J.; El Nahhas, A.; Lima, F. A.; Pham, V.-T.; Best, J.; Weinstein, J. A.; Borca, C. N.; Abela, R.; Bressler, C.; Chergui, M. *Angew. Chem., Int. Ed.* **2009**, *48*, 2711−2714.
(20) Penfold, T. J.; Curchod, B. F. E.; Tavernelli, I.; Abela, R.; Rothlisberger, U.; Chergui, M. *Phys. Chem. Chem. Phys.* **2012**, *14*, 9444−9450.
(21) Che, C. M.; Butler, L. G.; Gray, H. B.; Crooks, R. M.; Woodruff, W. H. *J. Am. Chem. Soc.* **1983**, *105*, 5492−5494.
(22) Stoyanov, S. R.; Villegas, J. M.; Rillema, D. P. *J. Phys. Chem. B* **2004**, *108*, 12175−12180.
(23) Novozhilova, I. V.; Volkov, A. V.; Coppens, P. *J. Am. Chem. Soc.* **2003**, *125*, 1079−1087.
(24) Shimizu, Y.; Tanaka, Y.; Azumi, T. *J. Phys. Chem.* **1984**, *88*, 2423−2425.
(25) Winkler, J. R.; Marshall, J. L.; Netzel, T. L.; Gray, H. B. *J. Am. Chem. Soc.* **1986**, *108*, 2263−2266.
(26) McCleskey, T. M.; Winkler, J. R.; Gray, H. B. *J. Am. Chem. Soc.* **1992**, *114*, 6935−6937.
(27) Caspar, J. V.; Gray, H. B. *J. Am. Chem. Soc.* **1984**, *106*, 3029−3030.
(28) King, C.; Auerbach, R. A.; Fronczek, F. R.; Roundhill, D. M. *J. Am. Chem. Soc.* **1986**, *108*, 5626−5627.
(29) Roundhill, D. M.; Shen, Z. P.; King, C.; Atherton, S. J. *J. Phys. Chem.* **1988**, *92*, 4088−4094.
(30) Fordyce, W. A.; Brummer, J. G.; Crosby, G. A. *J. Am. Chem. Soc.* **1981**, *103*, 7061−7064.
(31) Pan, Q.-J.; Fu, H.-G.; Yu, H.-T.; Zhang, H.-X. *Inorg. Chem.* **2006**, *45*, 8729−8735.
(32) Peterson, J. R.; Kalyanasundaram, K. *J. Phys. Chem.* **1985**, *89*, 2486−2492.
(33) An additional low-amplitude 60−290 ps decay component revealed by deconvolution of the TCSPC data (Table S2) is tentatively attributed to relaxation processes.
(34) Yersin, H.; Finkenzeller, W. J. In *Highly Efficient OLEDs with Phosphorescent Materials*; Wiley-VCH: Weinheim, 2008; pp 1−97.
(35) Yersin, H.; Rausch, A. F.; Czerwieniec, R.; Hofbeck, T.; Fischer, T. *Coord. Chem. Rev.* **2011**, *255*, 2622−2652.
(36) Baková, R.; Chergui, M.; Daniel, C.; Vlček, A., Jr.; Záliš, S. *Coord. Chem. Rev.* **2011**, *255*, 975−989.
(37) Siddique, Z. A.; Yamamoto, Y.; Ohno, T.; Nozaki, K. *Inorg. Chem.* **2003**, *42*, 6366−6378.
(38) Lawetz, V.; Orlandi, G.; Siebrand, W. *J. Chem. Phys.* **1972**, *56*, 4058−4072.
(39) Siebrand, W. *Chem. Phys. Lett.* **1970**, *6*, 192−194.
(40) Hager, G. D.; Crosby, G. A. *J. Am. Chem. Soc.* **1975**, *97*, 7031−7037.
(41) Gawelda, W.; Cannizzo, A.; Pham, V.-T.; van Mourik, F.; Bressler, C.; Chergui, M. *J. Am. Chem. Soc.* **2007**, *129*, 8199−8206.
(42) Cannizzo, A.; van Mourik, F.; Gawelda, W.; Zgrablic, G.; Bressler, C.; Chergui, M. *Angew. Chem., Int. Ed.* **2006**, *45*, 3174−3176.
(43) Cannizzo, A.; Blanco-Rodríguez, A. M.; Nahhas, A.; Šebera, J.; Záliš, S.; Vlček, A., Jr.; Chergui, M. *J. Am. Chem. Soc.* **2008**, *130*, 8967−8974.
(44) El Nahhas, A.; Cannizzo, A.; van Mourik, F.; Blanco-Rodríguez, A. M.; Záliš, S.; Vlček, A., Jr.; Chergui, M. *J. Phys. Chem. A* **2010**, *114*, 6361−6369.
(45) El Nahhas, A.; Consani, C.; Blanco-Rodríguez, A. M.; Lancaster, K. M.; Braem, O.; Cannizzo, A.; Towrie, M.; Clark, I. P.; Záliš, S.; Chergui, M.; Vlček, A., Jr. *Inorg. Chem.* **2011**, *50*, 2932−2943.
(46) Cho, S.; Mara, M. W.; Wang, X.; Lockard, J. V.; Rachford, A. A.; Castellano, F. N.; Chen, L. X. *J. Phys. Chem. A* **2011**, *115*, 3990−3996.
(47) Miskowski, V. M.; Rice, S. F.; Gray, H. B.; Dallinger, R. F.; Milder, S. J.; Hill, M. G.; Exstrom, C. L.; Mann, K. R. *Inorg. Chem.* **1994**, *33*, 2799−2807.
(48) Miskowski, V. M.; Rice, S. F.; Gray, H. B.; Milder, S. J. *J. Phys. Chem.* **1993**, *97*, 4277−4283.
(49) Marshall, J. L.; Stobart, S. R.; Gray, H. B. *J. Am. Chem. Soc.* **1984**, *106*, 3027−3029.
(50) Miskowski, V. M.; Goldbeck, R. A.; Kliger, D. S.; Gray, H. B. *Inorg. Chem.* **1979**, *18*, 86−89.
(51) Hopkins, M. D.; Gray, H. B. *J. Am. Chem. Soc.* **1984**, *106*, 2468.
(52) Alberding, B. G.; Chisholm, M. H.; Gustafson, T. L. *Inorg. Chem.* **2012**, *51*, 491−498.
(53) Byrnes, M. J.; Chisholm, M. H.; Gallucci, J. A.; Liu, Y.; Ramnauth, R.; Turro, C. *J. Am. Chem. Soc.* **2005**, *127*, 17343−17352.
(54) Alberding, B. G.; Chisholm, M. H.; Gallucci, J. C.; Ghosh, Y.; Gustafson, T. L. *Proc. Natl. Acad. Sci. U.S.A.* **2011**, *108*, 8152−8156.
(55) Siddique, Z. A.; Ohno, T.; Nozaki, K. *Inorg. Chem.* **2004**, *43*, 663−673.
(56) Hopkins, M. D.; Gray, H. B.; Miskowski, V. M. *Polyhedron* **1987**, *6*, 705−714.
(57) Benard, M.; Veillard, A. *Chem. Phys. Lett.* **1982**, *90*, 160−165.
(58) Lam, Y. C.; Labinger, J. A.; Bercaw, J. E.; Gray, H. B. Manuscript in preparation.
(59) Yasuda, N. .; Uekusa, H. .; Ohashi, Y. *Bull. Chem. Soc. Jpn.* **2004**, *77*, 933−944.